Journal of
Synchrotron
Radiation

ISSN 0909-0495

Received 12 December 2011
Accepted 16 May 2012

Extreme-ultraviolet compact spectrometer for the characterization of the harmonics content in the free-electron-laser radiation at FLASH

Fabio Frassetto,[a]* Stefano Coraggia,[a] Siarhei Dziarzhytski,[b] Natalia Gerasimova[b] and Luca Poletto[a]

[a]Institute of Photonics and Nanotechnologies, National Research Council of Italy, via Trasea 7, Padova 35131, Italy, and [b]HASYLAB, DESY, Notkestrasse 85, 22607 Hamburg, Germany. E-mail: frassett@dei.unipd.it

The design and the commissioning results of a portable and compact spectrometer for the high harmonics content characterization of the extreme-ultraviolet radiation of FLASH (free-electron laser in DESY, Hamburg, Germany) are presented. The instrument is a grazing-incidence flat-field spectrometer equipped with two variable-line-spaced gratings; it covers the 2–40 nm wavelength region with a spectral resolution in the 0.1–0.2% range. Both spectral and intensity fluctuations of the fundamental emission and the harmonics are monitored.

Keywords: grazing-incidence spectrometer; free-electron laser; extreme-ultraviolet.

1. Introduction

Free-electron-lasers (FELs) in the extreme-ultraviolet (XUV) and X-ray spectral regions are sources that can generate spatially coherent radiation, ultrashort time duration and an increase of six to eight orders of magnitude on the peak brilliance over third-generation synchrotron radiation (Saldin *et al.*, 2000; Khan, 2008). They are considered an indispensable tool for investigations spanning a very large horizon of experiments, such as pump-and-probe measurements, single-shot holography, dilute sample spectroscopy and solid investigations. Up to now around 20 FELs are in operation or scheduled (http://sbfel3.ucsb.edu/www/vl_fel.html).

In this framework, FLASH at DESY (Hamburg, Germany) has been the first user-dedicated FEL facility operated in the XUV. Since 2005 it has been providing intense, ultra-short and coherent radiation in the 6–47 nm wavelength range (Ackermann *et al.*, 2007). In 2009 the conclusion of a major upgrade drastically improved the capability of the machine, permitting photons to be obtained at wavelengths shorter than 5 nm at the first FEL harmonic.

As a rule of thumb, the more sophisticated the source, the more important the control of its characteristics. A suitable photon diagnostic system, capable of single-shot monitoring of the beam spectral features, is considered as an essential part of any FEL facility (Nicolosi *et al.*, 2005; Tiedtke *et al.*, 2009; Frassetto *et al.*, 2008; Zangrando *et al.*, 2009). The measurement of the FEL photon spectrum is required not only to tune the machine but also by the experiments that do not need to monochromatize the FEL radiation to avoid any temporal broadening of the pulse or reduction of photon flux, but do need knowledge of the spectral distribution of the FEL pulses.

We present here the design and characterization of a compact and portable spectrometer for the on-line monitoring of the FEL spectral features at the FLASH facility (DESY, Hamburg), in particular the content of high harmonics. The instrument mounts two spherical varied-line-spaced gratings to cover the 2–40 nm spectral region. The optical configuration is well known in the literature (Kita *et al.*, 1983; Nakano *et al.*, 1984; Harada *et al.*, 1999). The novelty of this diagnostic tool is the acquisition of the FEL spectral content in the experimental chamber in single-shot operation. Being compact, this tool can be easily placed behind a generic experimental set-up and can be used to monitor the single-shot spectral fluctuations of the beam. We emphasize that such a characterization is essential in order to optimize the self-amplified spontaneous emission process, and consequently, the experimental conditions.

2. The spectrometer

The instrumental concept is based on the use of spherical varied-line-spaced grazing-incidence gratings to realise a flat-field spectrometer, in which the spectral focal curve is almost parallel to the normal to the grating surface and almost flat, as presented in detail by Kita *et al.* (1983). The optical concept is shown in Fig. 1; the mechanical envelope and the instrument are shown in Fig. 2. The spectrometer is designed to be placed after the experimental station at the end of the FEL beamline, at a distance between 1 and 3 m behind the FEL focal point. The entrance slit, which limits the entering beam, acts as the spatial filtered source whose spectral components are dispersed and focused by the grating into the focal plane. A

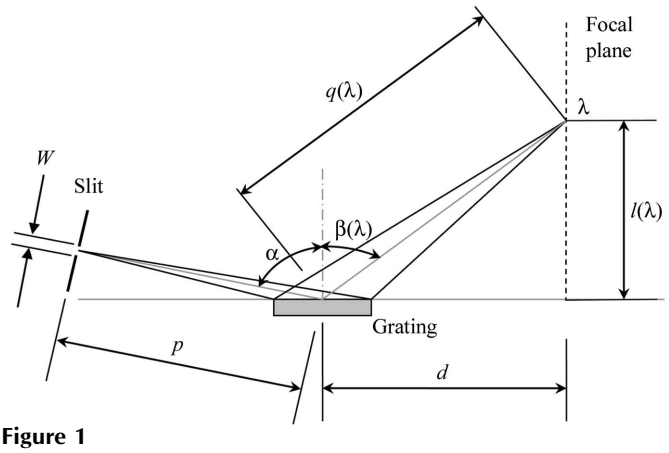

Figure 1
Instrumental optical concept.

proper choice of the parameters of the law for the groove density variation along the grating surface gives a focal plane that is ideally parallel to the normal to the grating center. The whole spectral range of operation spans from 2 to 40 nm and is fully covered using two gratings (manufactured by Hitachi, Japan) mounted on a motorized rotation stage that is used to select one of them. The gratings have the same input arm and share an overlying spectral focal curve. The grating parameters are listed in Table 1.

The length of the spectral focal curve in the whole range of operation is about 66 mm, which cannot be simultaneously covered by a single detector. Therefore the detector is mounted on a linear motorized translation stage that is connected to the grating vacuum chamber by an edge-welded bellow, 63 mm in diameter. The detector is moved along the spectral curve to acquire the spectral region of interest. The instrument is compatible with the ultra-high-vacuum requirements to be operated at FLASH. The requirement to move the detector to cover the whole spectral range limits the band where the FEL fundamental and its harmonics can be detected simultaneously. The spectral coverage for three detector positions is reported in Fig. 3.

Table 1
Grating parameters.

	G1200	G2400
Spectral range (nm)	5–40	2–20
Central groove density (mm^{-1})	1200	2400
Radius (mm)	5650	15920
Entrance arm p (mm)	237	
Incidence angle (°)	87	88.65
Distance d (mm)	235.3	
Accepted angle (mrad)	10 (spectral) × 10	5 (spectral) × 10

The installation of the spectrometer in different beamlines requires a simple and reliable alignment procedure. For this purpose two screens are mounted on a motorized linear stage in front of the gratings and can be inserted into the beam path between the entrance slit and the gratings. A phosphor target is used to align the spectrometer with the visible laser beam available at FLASH to visualize the XUV FEL path; a YAG:Ce crystal is used to detect the XUV FEL radiation. The two reference points that identify univocally the correct input

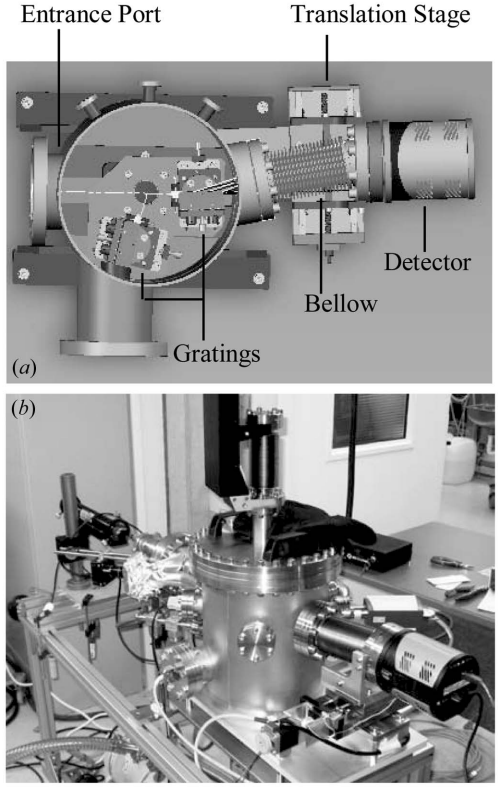

Figure 2
(*a*) Three-dimensional model of the spectrometer. (*b*) Photograph of the instrument.

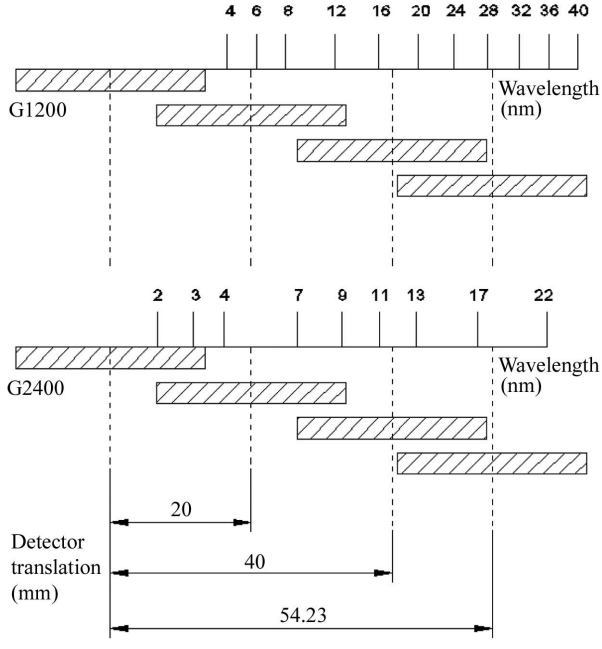

Figure 3
Spectral coverage for three detector positions. The dashed region represents the detector extension, which in our case is about 27 mm.

Table 2
Detector parameters.

Format	1340 × 400
Pixel size (μm)	20 × 20
Imaging area (mm)	26.8 × 8
Digitalization	16 bits
Full well capacity (ke^-)	300
Readout noise (e^-)	3.5 at 100 kHz

direction on the spectrometer are the entrance slit and the marker on the screen.

Let us indicate with $l(\lambda)$ the distance between the spectral position of a generic wavelength λ on the focal plane H and the intersection between the tangent to the grating surface at the grating center and the focal plane H, as shown in Fig. 1. The diffracted wavelength is calculated by the equation

$$\lambda = \frac{\sin\alpha - \sin\left[\tan^{-1}(d/l)\right]}{m\sigma}, \qquad (1)$$

where α is the incidence angle, m is the diffraction order and σ is the central groove density.

In the following the analysis will be restricted to the 2–20 nm region, this being the most used interval at FLASH.

The detector is a thinned back-illuminated XUV-enhanced CCD camera (model PIXIS-XO:400B provided by Princeton Instrument, USA). Its main parameters are resumed in Table 2. The CCD works in the almost single-photon-counting regime, since the silicon quantum yield (*i.e.* the number of electrons generated by an interacting photon) spans a range between 8 e^- at 40 nm and 170 e^- at 2 nm, which is higher than the CCD readout noise. The ratio between the full well capacity and the quantum yield is a measure of the detector dynamic range. It varies in the range between 37500 (at 40 nm) and 1700 (at 2 nm). The demand for a high dynamic range comes from the very high intensity variation between the harmonics. For a more flexible use, the detector provides two acquisition modes: low noise and high capacity; in the second case the gain (e^-/ADU) is about three times that in the first one.

3. Optical performances

The main parameters driving the instrumental performances, in terms of resolution, are the slit width W and the distance between the slit and the FEL focus, assuming that the size of the FEL spot is smaller than the slit aperture. Let us consider a working condition in which the slit is placed 1 m away from the FEL focus with an aperture of 100 μm. Under these conditions the beam divergence entering the instrument is about 100 μrad. Actually, the distance of the slit from the FEL focus may be longer than 1 m and the slit aperture may be narrower than 100 μm; consequently the divergence is even smaller than what has been assumed above. At these small values of divergence all the optical aberrations, mainly defocusing, coma and spherical aberration, can be neglected. Therefore, the slit image W' in the focal plane is related to the slit width W by the relation

$$W'(\lambda) = W\,\frac{q(\lambda)}{p}\,\frac{\cos\alpha}{\cos\beta(\lambda)}, \qquad (2)$$

where $q(\lambda)/p$ is the geometric magnification factor and $\cos\alpha/\cos\beta(\lambda)$ is the anamorphic magnification factor. The symbols are defined in Fig. 1: p is the entrance arm, $q(\lambda)$ the exit arm at wavelength λ, α the incidence angle and $\beta(\lambda)$ the diffraction angle.

W' is found to be smaller than the CCD pixel size over the whole spectral region of operation for any slit width below 50 μm for the G1200 grating and 100 μm for the G2400 grating.

The spectral resolving element, defined here as the ratio between the spectral interval covered by the single pixel and the wavelength, is shown in Fig. 4. The requirements on the resolution requested by the users, *i.e.* a resolution better than 0.25% over the whole spectral region of operation, are fulfilled.

Since the spectrometer has no focusing capabilities in the direction parallel to the slit, the divergence of the beam in that direction is the same as the FEL beamline; therefore the height of the image on the detector may be used to measure the beam divergence at the different wavelengths.

4. Calibration

The grating efficiencies have been measured at CNR-IFN Padova (Italy) and at the beamline BEAR at the ELETTRA synchrotron (Trieste, Italy). The gratings G1200 and G2400 have been characterized in their nominal spectral region of

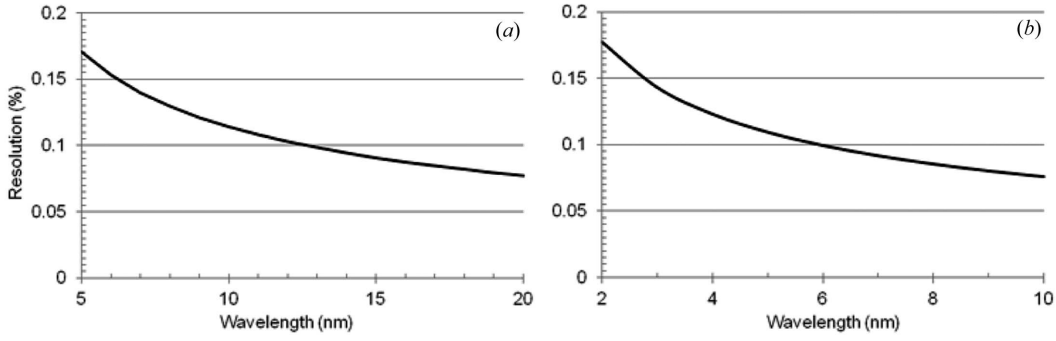

Figure 4
Spectral extension of the resolving element (20 μm pixel size). (*a*) G1200, (*b*) G2400.

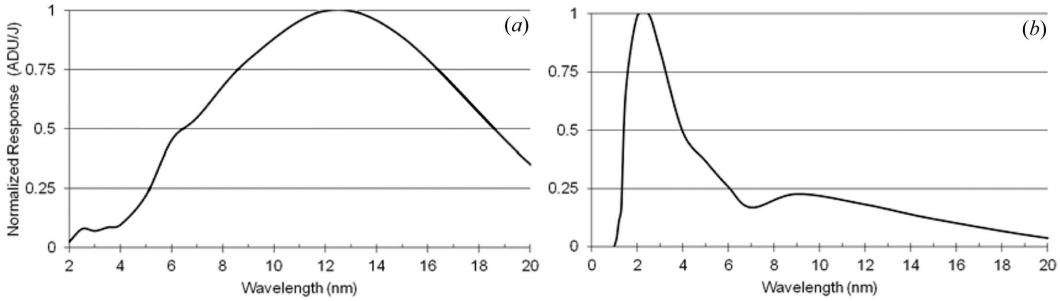

Figure 5
Spectrometer total response $R(\lambda)$: (*a*) G1200; (*b*) G2400. The curves are normalized to unity and represent the digital signal (ADU) measured on the CCD (with the spectrometer gratings operated at the first diffraction order) and produced by an incident photon flux of 1 J.

operation as shown in Table 1, showing, respectively, a peak efficiency of 18% at 12 nm and 2.2% and 3 nm.

The instrumental global response has been measured at beamline BW3 at the DORIS synchrotron (Hamburg, Germany) using a calibrated AXUV photodiode (provided by International Radiation Detectors, USA) as the reference detector. The calibration procedure is based on the comparison, at a fixed wavelength, between the signal diffracted at the first order on the CCD and the signal read by the photodiode positioned behind the entrance slit. The total response of the spectrometer $R(\lambda)$ is shown in Fig. 5 for both gratings.

The spectrometer relative efficiency at the different grating diffraction orders for the grating G1200 is plotted in Fig. 6; the curves are normalized to the signal at the first diffraction order. The grating shows a clear increase in the efficiency of the high orders at wavelengths around 4 nm. The G2400 grating, differently, has a second-order efficiency that is $<10\%$ of the first one in its working region.

5. Spectral characterization of FLASH: high harmonics and beam divergence

The commissioning phase was carried out in August 2010. In four time slots FLASH was tuned to four different wavelengths: 6.8 nm, 13.0 nm, 19.2 nm and 25.6 nm. The spectrometer was placed at the end of BL1, 3.5 m behind the focus of the beamline; see Fig. 7. This arrangement reflects the typical insertion layout planned for the instrument: the distance between the focal spot and the entrance slit ensures the possibility of easily inserting an experiment at the FEL focal spot.

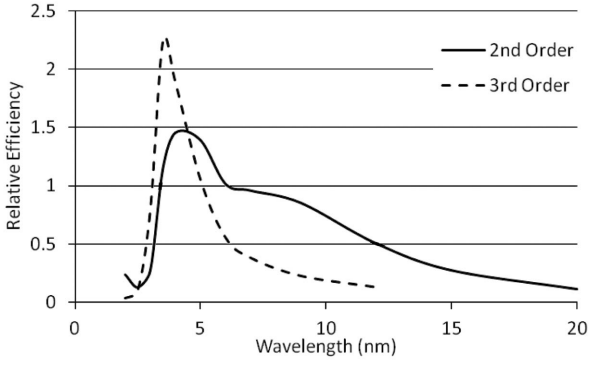

Figure 6
Relative efficiency of the spectrometer at different grating diffraction orders. The curves are normalized to the first-order efficiency and are referred to the grating G1200.

The acquired data have permitted the analysis of three different characteristics of the FEL radiation: (i) average and single-shot content of high harmonics with respect to the fundamental, (ii) spectrum and (iii) divergence. In this paper we present the results obtained at the two wavelengths 6.8 nm and 19.2 nm.

The relative harmonic content has been measured using the procedure described in the following. The signal integrated over the whole spectral line (once the noise level has been subtracted) is a measure of the photon flux passing through the slit. The latter, being placed far away from the FEL focus, limits the amount of photons entering the spectrometer, as schematically shown in Fig. 8.

We have to estimate the percentage of the total flux that is transmitted through the entrance slit. Let us suppose that the beam on the slit plane has a Gaussian symmetrical shape, described as

$$A(x, y) = K \exp\left[-\left(x^2 + y^2\right)/2\sigma^2\right], \qquad (3)$$

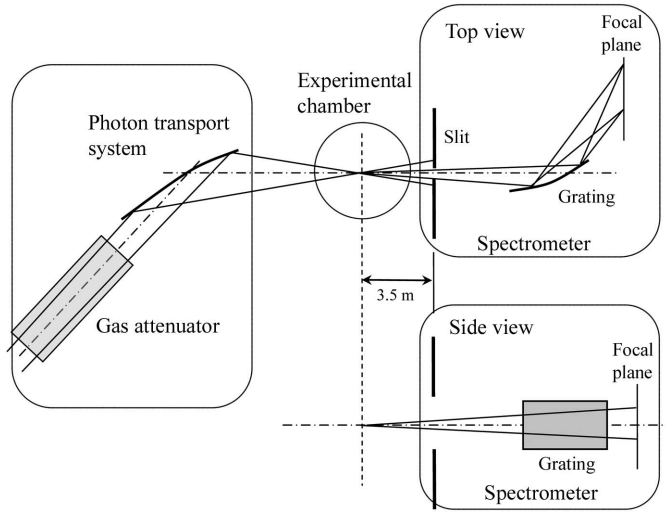

Figure 7
Scheme of the optical arrangement used during the commissioning phase.

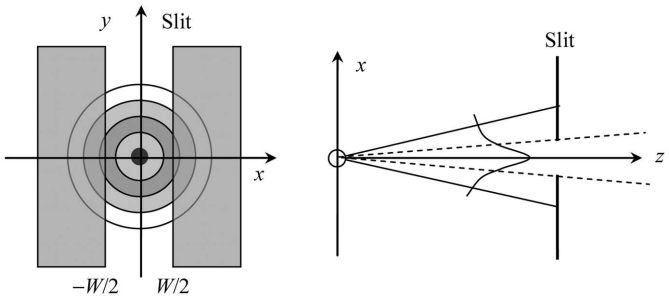

Figure 8
Effect of the slit on the FEL beam, supposed to have a two-dimensional Gaussian shape at the entrance plane of the spectrometer. The slit aperture is W, and only the beam between $-W/2$ and $W/2$ in the x direction is transmitted.

where x and y are the transverse coordinates, y being parallel to the slit. The Gaussian width σ is calculated from the line profile acquired on the CCD along the y direction.

The slit is supposed to limit the flux only in the x direction, therefore the ratio between the intensity passing through the slit and the total intensity is

$$T_{\rm SLIT}(W,\sigma) = \mathrm{erf}\left(\frac{W}{2\sqrt{2}\sigma}\right) = \frac{2}{\sqrt{\pi}} \int_0^{W/(2\sqrt{2}\sigma)} \exp\left(-\xi^2\right) \mathrm{d}\xi, \quad (4)$$

where W is the slit width and erf indicate the Gauss error function.

The FEL signal in the experimental chamber, $S(\lambda)$, is finally calculated as

$$S(\lambda) = S_{\rm CCD}(\lambda)/\left[T_{\rm SLIT}(W,\sigma)\, R(\lambda)\right], \quad (5)$$

where $S_{\rm CCD}(\lambda)$ is the signal integrated on the CCD on the whole spectral line centred at wavelength λ, $R(\lambda)$ is the normalized response of the spectrometer and $T_{\rm SLIT}$ is calculated from equation (4).

$S(\lambda)$ does not indicate the absolute photon flux, since it is obtained through the normalized response $R(\lambda)$. It gives the relative intensity between the different spectral components of the FEL beam, in particular between the fundamental and the harmonics. Since the spectrometer is installed after the experimental chamber without interposing any additional optical element that may alter the relative spectral composition of the FEL beam, $S(\lambda)$ is the information that is directly provided to the users.

Furthermore, $S(\lambda)$ is acquired in a single-shot basis, therefore it also gives the measurement of the FEL spectral fluctuations (in accordance with the instrument resolution). Some spectra taken with the G2400 grating of the fundamental at 19.2 nm, the third and fifth harmonics, respectively, at 6.4 nm and 3.9 nm, are shown in Fig. 9.

If the total transmission of the different elements of the beamline is known as a function of the wavelength, $S(\lambda)$ may also be related to the signal emitted by the FEL source, $S_{\rm FEL}(\lambda)$, through the equation

$$S_{\rm FEL}(\lambda) = S(\lambda)/\left[T_{\rm GAS}(\lambda)\, T_{\rm BL}(\lambda)\right], \quad (6)$$

where $T_{\rm BL}(\lambda)$ is the transmission of the beamline, taking into account all of the optical elements, and in the considered case is due to the reflectivity of the optics, but in a more generic case can account for more complex effects, such as, for example, the throughput of a monochromator. $T_{\rm GAS}(\lambda)$ is the transmission of the gas attenuator cell; it is realised with a 15 m-long tube fillable with different gases at tunable pressures (Hahn & Tieke, 2007). The proper choice of the gas and the pressure may attenuate the strong fundamental FEL emission and transmit the harmonics, allowing the simultaneous measurement of all the spectral features. In addition, for different attenuation profiles, filter foils can be inserted just before the spectrometer entrance slit; in this case the right-hand term in equation (6) has to be divided by $T_{\rm FOIL}(\lambda)$. In the measurements that will be presented in the following, Ne at 0.005 mbar has been used to attenuate the fundamental at 19.2 nm, and Kr at 0.006 mbar for the fundamental at 6.8 nm.

The harmonic contents calculated at the end of the beamline, $S(\lambda)$, and at the source, $S_{\rm FEL}(\lambda)$, are shown in Fig. 10. The emission at the source has been calculated by using the transmission data of beamline BL1 and the attenuation of the gas cell under the operative conditions.

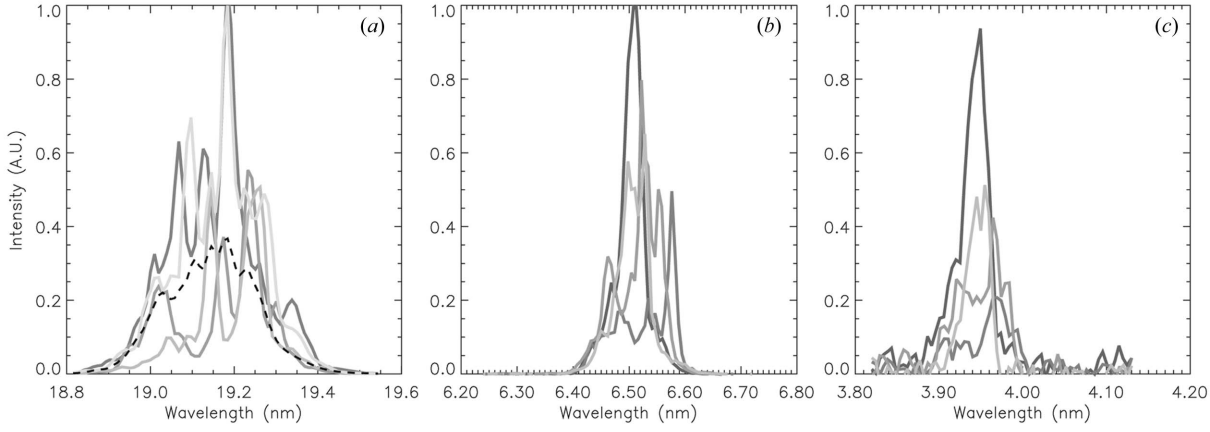

Figure 9
Shot-to-shot spectral fluctuation at the fundamental of 19.2 nm (*a*), at the third harmonic (*b*) and at the fifth harmonic (*c*). The three panels have different normalization factors. In (*a*) the dashed line represents the mean of 30 shots.

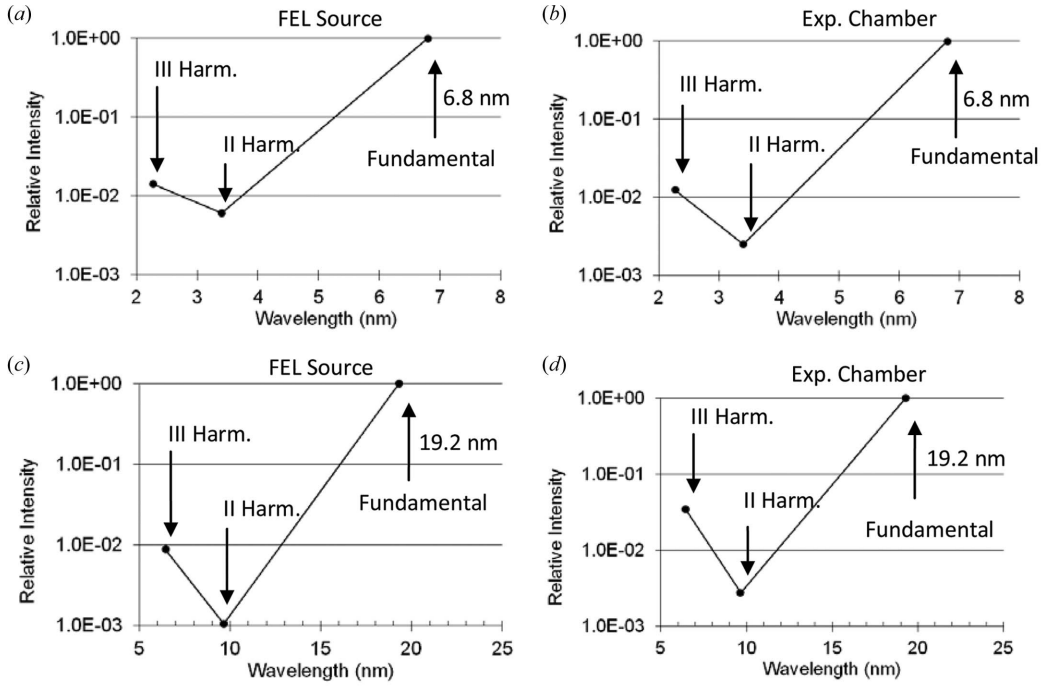

Figure 10
Relative harmonic content: (*a*, *b*) fundamental at 6.8 nm; (*c*, *d*) fundamental at 19.2 nm. (*a*, *c*) are the harmonic content $S_{\rm FEL}(\lambda)$ of the FEL source; (*b*, *d*) are referred to the signal $S(\lambda)$ in the experimental chamber. In both cases the IV harmonic was not measurable.

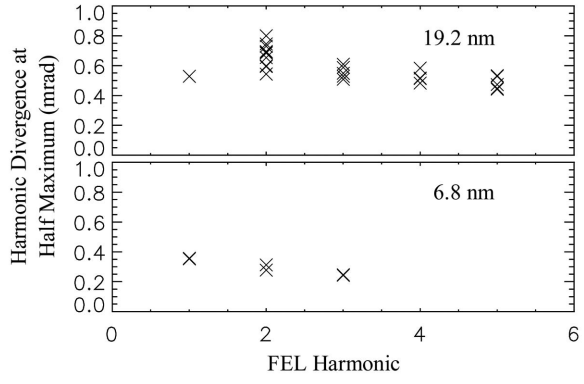

Figure 11
Beam divergence measured at the two considered fundamental wavelengths. Each panel is referred to a specific fundamental radiation and to its harmonics.

The third-harmonic emission is of the order of a few percent of the fundamental, as already reported in the literature (Ackermann *et al.*, 2007). It is worth noting that the amount of second harmonic is lower than that of the third harmonic: ideally, the second harmonic would vanish when the electron bunch propagates exactly on axis.

The measurement of the shape of the different spectral features on the CCD in the direction perpendicular to the spectral dispersion plane, associated with the known distance between the focus of the beamline and the CCD, gives the angular divergence of the beam in the direction parallel to the slit of the spectrometer. The divergence of the fundamental has been measured to be 0.53 mrad at 19.2 nm and 0.35 mrad at 6.8 nm. The values of the harmonics are shown in Fig. 11.

6. Conclusions

We have presented the design and characterization of a compact spectrometer for the monitoring of the spectral features of the radiation produced at the FLASH FEL. The instrument can be installed at the end of different beamlines through a reliable alignment procedure. The FEL characteristics that can be analyzed are the harmonic content with respect to the fundamental, the vertical beam divergence and the shot-to-shot spectral variation.

References

Ackermann, W., Asova, G., Ayvazyan, V., Azima, A., Baboi, N., Bähr, J., Balandin, V., Beutner, B., Brandt, A. & Bolzmann, A. (2007). *Nat. Photon.* **1**, 336–342.
Frassetto, F., Cocco, D., Zangrando, M. & Poletto, L. (2008). *Nucl. Instrum. Methods Phys. Res. A*, **593**, 129–131.
Hahn, U. & Tieke, K. (2007). *AIP Conf. Proc.* **879**, 276–282.
Harada, T., Takahashi, K., Sakuma, H. & Osyczka, A. (1999). *Appl. Opt.* **38**, 2743–2748.
Khan, S. (2008). *J. Mod. Opt.* **55**, 3469–3512.
Kita, T., Harada, T., Nakano, N. & Kuroda, H. (1983). *Appl. Opt.* **22**, 512–513.
Nakano, N., Kuroda, H., Kita, T. & Harada, T. (1984). *Appl. Opt.* **23**, 2386.
Nicolosi, P., Poletto, L., Pelizzo, M.-G., Epulandi, L., Zambolin, P., Feldhaus, J., Jastrow, U., Hahn, U., Ploenjes, E. & Tiedtke, K. (2005). *J. Electron Spectrosc. Relat. Phenom.* **144–147**, 1055–1058.
Saldin, E. L., Schneidmiller, E. A. & Yurkov, M. V. (2000). *The Physics of Free Electron Lasers.* Berlin: Springer.
Tiedtke, K., Azima, A., von Bargen, N., Bittner, L., Bonfigt, S., Düsterer, S., Faatz, B. & Frühling, U. (2009). *New J. Phys.* **11**, 023029.
Zangrando, M., Abrami, A., Bacescu, D., Cudin, I., Fava, C., Frassetto, F., Galimberti, A., Godnig, R., Giuressi, D., Poletto, L., Rumiz, L., Sergo, R., Svetina, C. & Cocco, D. (2009). *Rev. Sci. Instrum.* **80**, 113110.